

High winding number of topological phase in non-unitary periodic quantum walk

Yali Jia(贾雅利) and Zhi-Jian Li(李志坚)

Citation: Chin. Phys. B, 2021, 30 (**10**): 100301. DOI: 10.1088/1674-1056/abf554
Journal homepage: http://cpb.iphy.ac.cn; http://iopscience.iop.org/cpb

What follows is a list of articles you may be interested in

Superfluid states in α-T_3 lattice

Yu-Rong Wu(吴玉容) and Yi-Cai Zhang(张义财)
Chin. Phys. B, 2021, 30 (**6**): 060306. DOI: 10.1088/1674-1056/abea8a

Realization of arbitrary two-qubit quantum gates based on chiral Majorana fermions

Qing Yan(闫青) and Qing-Feng Sun(孙庆丰)
Chin. Phys. B, 2021, 30 (**4**): 040303. DOI: 10.1088/1674-1056/abe296

Metal-insulator phase transition and topology in a three-component system

Shujie Cheng(成书杰) and Xianlong Gao(高先龙)
Chin. Phys. B, 2021, 30 (**1**): 010302. DOI: 10.1088/1674-1056/abb305

The entanglement of deterministic aperiodic quantum walks

Ting-Ting Liu(刘婷婷), Ya-Yun Hu(胡亚运), Jing Zhao(赵静), Ming Zhong(钟鸣), Pei-Qing Tong(童培庆)
Chin. Phys. B, 2018, 27 (**12**): 120305. DOI: 10.1088/1674-1056/27/12/120305

Topological phase transitions driven by next-nearest-neighbor hopping in noncentrosymmetric cold Fermi gases

Wang Rui, Zhang Cun-Xi, Ji Qing-Shan
Chin. Phys. B, 2015, 24 (**3**): 030305. DOI: 10.1088/1674-1056/24/3/030305

High winding number of topological phase in non-unitary periodic quantum walk*

Yali Jia(贾雅利) and Zhi-Jian Li(李志坚)†

Institute of Theoretical Physics, Shanxi University, Taiyuan 030006, *China*

(Received 7 January 2021; revised manuscript received 10 March 2021; accepted manuscript online 7 April 2021)

Topological phases and their associated multiple edge states are studied by constructing a one-dimensional non-unitary multi-period quantum walk with parity-time symmetry. It is shown that large topological numbers can be obtained when choosing an appropriate time frame. The maximum value of the winding number can reach the number of periods in the one-step evolution operator. The validity of the bulk–edge correspondence is confirmed, while for an odd-period quantum walk and an even-period quantum walk, they have different configurations of the 0-energy edge state and π-energy edge state. On the boundary, two kinds of edge states always coexist in equal amount for the odd-period quantum walk, however three cases including equal amount, unequal amount or even only one type may occur for the even-period quantum walk.

Keywords: periodic quantum walk, high winding number, edge states

PACS: 03.67.Ac, 05.40.Fb, 03.65.Vf **DOI:** 10.1088/1674-1056/abf554

1. Introduction

Quantum walks (QWs) are the quantum analog of classical random walks,[1–3] where a walker propagates on a lattice and the direction of propagation is conditioned over the state of its coin. Compared with classical random walks, the mutual interference enhancement or cancellation of QWs on different propagating paths makes it exhibit many different dynamic behaviors,[2] for example, a quadratically fast spread of the walker over the lattice. Based on its superiorities, QWs are widely used in quantum computation,[4] quantum search algorithms,[5] quantum simulations,[6] and quantum state transfer.[7]

More recently, it is shown that a QW is a versatile simulator of some novel phenomena observed in condensed matter physics.[8] Particularly, the realization of topological phase using a discrete-time quantum walk has aroused great interests.[9–12] On aspects of experiments, QWs have been implemented in many physical systems such as nuclear magnetic resonance,[13–15] trapped atoms[16,17] and integrated optics.[18] Among of them, photonic quantum walks[19–21] offer a versatile platform to explore topological phenomena in the context of non-unitary dynamics due to the ease of adjusting gain and loss.[22–24] PT-symmetric QWs with alternating gain and loss have been investigated.[25–27]

For a Hermitian system, some states appearing in a band gap are the edge states at the boundary of two deferent topological phase regions. The bulk–edge correspondence predicts that the number of edge states is equal to the difference of topological numbers in two regions.[28,29] In non-Hermitian systems, however, the bulk–edge correspondence needs to further verify because two kinds of band gaps, point and line gaps, appear for complex energy.[30,31] Moreover, the enlarged symmetries in non-Hermitian systems also affect bulk–edge correspondence. In this work, we classify a multi-period QW with PT-symmetry into an odd-period QW and an even-period QW, and demonstrate the validity of the bulk–edge correspondence for the system with large winding number.

2. Periodic quantum walk

A discrete time quantum walk over a one-dimensional lattice is dominated by a time-evolution operator U, which is implemented by a concatenation of coin operation C and successive position shift S.[2] It takes place in the Hilbert space $\mathcal{H}_\mathcal{P} \otimes \mathcal{H}_\mathcal{C}$, where the position Hilbert $\mathcal{H}_\mathcal{P}$ is spanned by the position basis states $\{|x\rangle, x \in Z\}$, and the coin Hilbert space $\mathcal{H}_\mathcal{C}$ is spanned by the coin basis states $\{|\uparrow\rangle, |\downarrow\rangle\}$. Generally, the coin operator has the form $C = I_x \otimes R(\theta)$, where I_x is the unit operator, and $R(\theta)$ is the rotation operator in inner coin space,

$$R_\theta = \begin{pmatrix} \cos\theta & -\sin\theta \\ \sin\theta & \cos\theta \end{pmatrix}. \tag{1}$$

The shift operator S that translates the particle to the left and/or right conditioned on the internal state of the particles has the form

$$S = \sum_x |x+1\rangle\langle x| \otimes |\uparrow\rangle\langle\uparrow| + \sum_x |x-1\rangle\langle x| \otimes |\downarrow\rangle\langle\downarrow|. \tag{2}$$

A single step time evolution operator is given by

$$U = SC, \tag{3}$$

*Project supported by the National Natural Science Foundation of China (Grant No. 12004231).

†Corresponding author. E-mail: zjli@sxu.edu.cn

© 2021 Chinese Physical Society and IOP Publishing Ltd

and the state of quantum walker after t steps can be expressed as

$$|\Psi(t)\rangle = U^t |\Psi(0)\rangle = (SC)^t |\Psi(0)\rangle \tag{4}$$

for a given initial state $|\Psi(0)\rangle$. The major point of difference between the classical and quantum implementations of the discrete time walk is the use of a quantum, rather than classical, coin operator with the result that the walker now has the possibility of being in a superposition of possible coin states $|\uparrow\rangle$ and $|\downarrow\rangle$ at every step.

The periodic quantum walk is defined by using two coin operators $C(\theta_1)$ and $C(\theta_2)$. The single step evolution operator of the two-period quantum walk is

$$U_2 = SC(\theta_1)SC(\theta_2), \tag{5}$$

and of the three-period quantum walk is

$$U_3 = SC(\theta_1)SC(\theta_1)SC(\theta_2). \tag{6}$$

More generally, for the m-period quantum walk it is

$$U_m = (SC(\theta_1))^{m-1}SC(\theta_2). \tag{7}$$

The periodic quantum walk defined above can be realized in a quantum optical system, where the walker is shifted more than twice at each time step.[32] However, the optical signal in an optical system will experience gain or loss.[33] Thus, we introduce the gain and loss operator as follows:

$$G = \sum_x |x\rangle\langle x| \otimes \begin{pmatrix} \mathrm{e}^{\gamma} & 0 \\ 0 & \mathrm{e}^{-\gamma} \end{pmatrix}, \tag{8}$$

and construe the time evolution to be

$$\tilde{U}_m = G^{-1}(SC(\theta_1))^{m-1}GSC(\theta_2). \tag{9}$$

The G is a non-unitary operator when $\gamma \neq 0$, and consequently the time evolution operator U_m becomes non-unitary. If $\gamma > 0$, the non-unitary describes an amplified process for the walker's amplitude with coin state $|\uparrow\rangle$ and a simultaneously decayed process with coin state $|\downarrow\rangle$. G^{-1} has the reverse action with respect with G; γ is called the degree of non-unitary since the strength of amplification or loss increases as γ becomes larger and larger.

3. Topological properties of the non-unitary periodic quantum walk with PT symmetry

The topological phase for non-Hermitian Hamiltonians, especially with PT symmetry, has become a rapidly growing research field in the recent years.[10] A non-unitary two-period QW as a quantum simulator has been used to study the edge states of open quantum systems. In this paper, we focus on the topological phenomena of multi-period QWs with PT-symmetry.

3.1. Dispersion relation

Since the operator $\tilde{U}_m$ has translation invariance, performing the Fourier transform, $\tilde{U}_m$ in the momentum space is diagonal,

$$\tilde{U}_m = \int_{-\pi}^{\pi} \mathrm{d}k\, |k\rangle\langle k| \otimes \tilde{U}_m(k), \tag{10}$$

$$\tilde{U}_m(k) = d_{m0}(k)\sigma_0 + d_{m1}(k)\sigma_x + d_{m2}(k)\sigma_y + d_{m3}(k)\sigma_z, \tag{11}$$

where σ_i $(i = x, y, z)$ is the Pauli matrix, which is a two-dimensional identity matrix. From $\tilde{U}_m(k)\tilde{U}_m^{-1}(k) = 1$, we get that the coefficients $d_{mj}(k)$ $(j = 0, 1, 2, 3)$ satisfy the relation

$$d_{m0}{}^2(k) - d_{m1}{}^2(k) - d_{m2}{}^2(k) - d_{m3}{}^2(k) = 1. \tag{12}$$

The eigenvalues of $\tilde{U}_m(k)$ are given by

$$\lambda_{\pm}(k) = \mathrm{e}^{\pm \mathrm{i}E_m} = d_{m0}(k) \pm \mathrm{i}\sqrt{1 - d_{m0}(k)^2}. \tag{13}$$

To clarify the PT symmetry for the non-unitary QW, the symmetric time frame is introduced for the time evolution operator,[28] in which $\tilde{U}_m(k)$ is redefined as

$$\tilde{U}'_m(k) = C\left(\frac{\theta_2}{2}\right)G^{-1}[SC(\theta_1)]^{m-1}GSC\left(\frac{\theta_2}{2}\right). \tag{14}$$

It is easy to verify that the PT symmetry relation holds

$$(PT)\,\tilde{U}'_m(k)\,(PT)^{-1} = \tilde{U}'^{-1}_m(k), \tag{15}$$

where the PT symmetry operator has the form

$$PT = \sum_x |-x\rangle\langle x| \otimes \sigma_z \mathcal{K}, \tag{16}$$

with $\mathcal{K}$ being the complex conjugation operator. We state that an eigenstate of the PT-symmetry time evolution operator $\tilde{U}'_m(k)$ spontaneously breaks PT-symmetry if it is not the eigenstate of the PT operator. In the PT-symmetry regime, the quasi-energy are real and $|\lambda| = 1$.[34] Otherwise, some quasi-energy becomes complex and $|\lambda| \neq 1$ in the PT-symmetry broken regime.

In the following we use three-period and four-period QWs as an example to investigate the topological properties of the odd-period and even-period QWs. After some calculation, we obtain the coefficients d_{mj} in Eq. (11) as follows:

$$\begin{aligned}
d_{30}(k) &= -\left[\cos\theta_2 \sin^2\theta_1 + \sin\theta_2 \sin(2\theta_1)\cosh(2\gamma)\right]\cos k \\
&\quad + \cos\theta_2 \cos^2\theta_1 \cos(3k), \\
d_{31}(k) &= \sin(2\theta_1)\sinh(2\gamma)\cos k, \\
d_{32}(k) &= \mathrm{i}\left[-\sin\theta_2 \sin^2\theta_1 + \cos\theta_2 \sin(2\theta_1)\cosh(2\gamma)\right]\cos k \\
&\quad + \mathrm{i}\sin\theta_2 \cos^2\theta_1 \cos(3k), \\
d_{33}(k) &= \mathrm{i}\sin^2\theta_1 \sin k - \mathrm{i}\cos^2\theta_1 \sin(3k)
\end{aligned} \tag{17}$$

for the non-unitary three-period QW $\tilde{U}_3'$. For the non-unitary four-period QW $\tilde{U}_4'$, they are

$$\begin{aligned}
d_{40}(k) &= \cos\theta_2[\cos(3\theta_1)\cos^2 k\cos(2k) \\
&\quad -\cos\theta_1\sin^2 k(2+3\cos(2k))] \\
&\quad -\cosh(2\gamma)\sin\theta_1\sin\theta_2\left[\cos(2k)+2\cos^2 k\cos(2\theta_1)\right], \\
d_{41}(k) &= \sinh(2\gamma)\left(\sin(3\theta_1)\cos^2 k-\sin\theta_1\sin^2 k\right), \\
d_{42}(k) &= \mathrm{i}\cos\theta_2\cosh(2\gamma)\left[\cos(3\theta_1)\cos^2 k-\sin\theta_1\sin^2 k\right] \\
&\quad +\mathrm{i}\sin\theta_2[\cos(3\theta_1)\cos^2 k\cos(2k) \\
&\quad -\cos\theta_1\sin^2 k(2+3\cos(2k))], \\
d_{43}(k) &= -\mathrm{i}\cos^3\theta_1\sin(4k)+2\mathrm{i}\cos\theta_1\sin^2\theta_1\sin(2k). \qquad (18)
\end{aligned}$$

When $\gamma = 0.1$, Figs. 1(a)–1(d) and 1(e)–1(h) present the energy dispersion relations under different coin parameters (θ_1, θ_2) for the non-unitary three-period QW and the four-period QW, respectively. The real part of E_m is shown by the black solid curves and its imaginary part is shown by the red dashed curves. As shown in Figs. 1(a), 1(b), and 1(e), the quasi-energy is real and the gap does not close. The eigenstate of the non-unitary time evolution preserves PT symmetry. However, in Figs. 1(c)–1(d), the quasi-energy becomes complex at some values of momentum, at which the eigenstate breaks PT symmetry. Correspondingly, the gap of the real part closes into a line segment with $\mathrm{Re}(E_3) = 0$ and π. The number of gap-closed line segments with $\mathrm{Re}(E_3) = 0$ is equal to that with $\mathrm{Re}(E_3) = \pi$. The above situation can also appear for the four-period QW. More interestingly, Fig. 1(f) shows that the number of gap-closed line segments with $\mathrm{Re}(E_3) = 0$ is not equal to that with $\mathrm{Re}(E_3) = \pi$. Even the gap closes only with $\mathrm{Re}(E_3) = \pi$ in Fig. 1(g), and closes only with $\mathrm{Re}(E_3) = 0$ in Fig. 1(h). These three situations do not appear for the three-period QW.

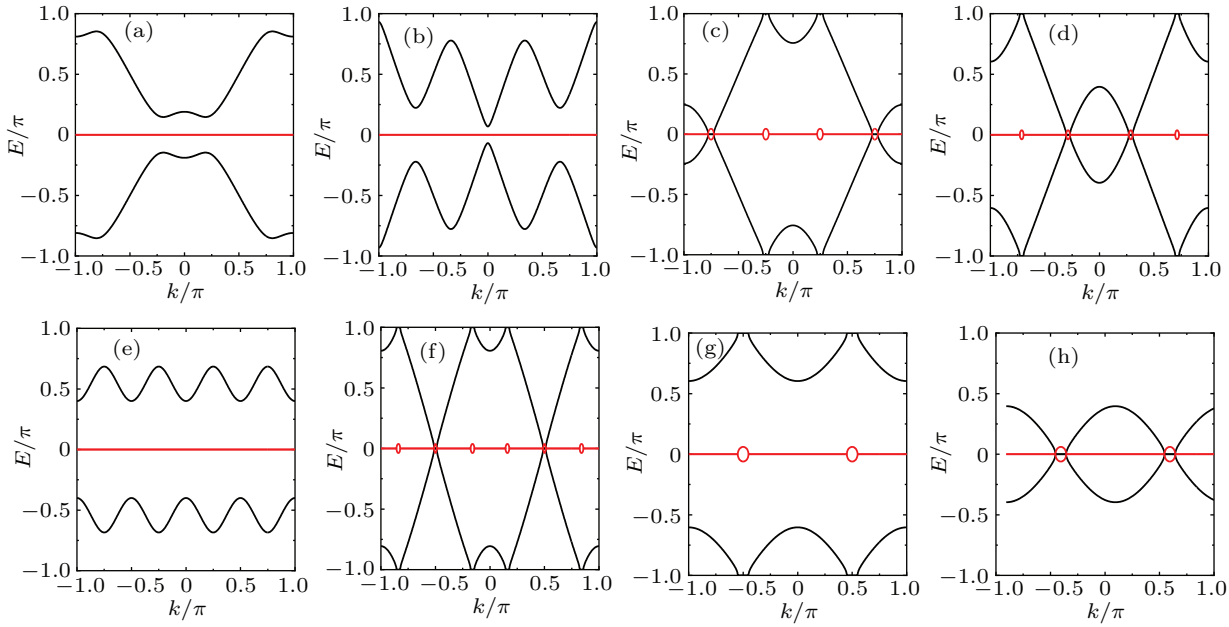


Fig. 1. The dispersion relation diagrams of the non-unitary three-period quantum walk (up pattern) and the four-period quantum walk (down pattern) for different values of (θ_1, θ_2): (a) $(\theta_1, \theta_2) = (-4\pi/5, -3\pi/5)$, (b) $(\theta_1, \theta_2) = (-\pi/10, \pi/8)$, (c) $(\theta_1, \theta_2) = (\pi/4, \pi/4)$, (d) $(\theta_1, \theta_2) = (4\pi/5, 4\pi/5)$, (e) $(\theta_1, \theta_2) = (-4\pi/5, -4\pi/5)$, (f) $(\theta_1, \theta_2) = (-\pi/5, \pi/5)$, (g) $(\theta_1, \theta_2) = (-3\pi/5, 2\pi/5)$, (h) $(\theta_1, \theta_2) = (-2\pi/5, 2\pi/5)$.

In general, the band gap closes equally with both $\mathrm{Re}(E_m) = 0$ and π for the odd-period QW, while for the even-period QW the number of gap-closed line segments with $\mathrm{Re}(E_m) = 0$ and π may be unequal. The reasons why the results obtained from the three-period QW and the four-period QW can be generalized to the universal odd-period QW and even-period QW are given in the following. For the odd-period QW, the time-evolution operator $\tilde{U}_m$ changes the positions of the walker from odd (even) sites to even (odd) sites at every iteration. By changing the order of the basis to separate even and odd sites, $\tilde{U}_m$ is described as the anti-block diagonal form

$$\tilde{U}_m = \begin{pmatrix} 0 & \tilde{U}_{\mathrm{e}}^{\mathrm{o}} \\ \tilde{U}_{\mathrm{o}}^{\mathrm{e}} & 0 \end{pmatrix}. \qquad (19)$$

It is found that $\tilde{U}_m$ satisfies the relation

$$\tau_m \tilde{U}_m \tau_m = -\tilde{U}_m, \qquad (20)$$

where $\tau_m = \begin{pmatrix} I & 0 \\ 0 & -I \end{pmatrix}$ and I denotes the identity operator that has the same dimension as $\tilde{U}_{\mathrm{e}}^{\mathrm{o}}$ and $\tilde{U}_{\mathrm{o}}^{\mathrm{e}}$. This relation guarantees the existence of an eigenstate with eigenvalue $\mathrm{e}^{-\mathrm{i}(E_m+\pi)}$ if and only if $\tilde{U}_m$ has the eigenstate with eigenvalue $\mathrm{e}^{-\mathrm{i}E_m}$. Hence the band gap closes at $\mathrm{Re}(E_m) = 0$ and $\mathrm{Re}(E_m) = \pi$ simultaneously. For the even-period QW, the time-evolution operator $\tilde{U}_m$ changes the positions of the walker from odd (even) sites to odd (even) sites at every iteration. Therefore, the matrix of $\tilde{U}_m$ in the basis arranging in the order of odd and even

sites is diagonal,

$$\tilde{U}_m = \begin{pmatrix} \tilde{U}_{\rm e}^{\rm e} & 0 \\ 0 & \tilde{U}_{\rm o}^{\rm o} \end{pmatrix}. \tag{21}$$

We can obtain the relation $\tau_m \tilde{U}_m \tau_m = \tilde{U}_m$, which does not enforce the constraint on the relation of 0-energy states and π-energy states.

3.2. Characterizing topological phases

Because the time evolution operator is a non-unitary operator, we cannot calculate winding numbers in an ordinary way. We characterize topological phases using topological numbers given by the global Berry phase.[24] The global Berry phase $\varphi_{\rm B}$ is defined as

$$\begin{aligned} \varphi_{m\rm B} &= \varphi_{m+} + \varphi_{m-}, \\ \varphi_{m\pm} &= -{\rm i}\oint {\rm d}k \frac{\langle \chi_{m\pm}| \frac{\rm d}{{\rm d}k} |\psi_{m\pm}\rangle}{\langle \chi_{m\pm}|\psi_{m\pm}\rangle}. \end{aligned} \tag{22}$$

where $\langle \chi_{m\pm}|$ and $|\psi_{m\pm}\rangle$ denote left and right eigenvectors of a non-unitary time evolution operator $\tilde{U}'_m$ with the eigenvalues $\lambda_{m\pm}$, respectively. It is straightforward to derive

$$|\psi_{m\pm}\rangle = \frac{1}{\sqrt{2D_m^2 \pm 2d_{m3}D_m}} \begin{pmatrix} d_{m1} - {\rm i}d_{m2} \\ \pm D_m - d_{m3} \end{pmatrix},$$
$$|\chi_{m\pm}\rangle = \frac{1}{\sqrt{2D_m^2 \pm 2d_{m3}D_m}} \begin{pmatrix} d^*_{m1} - {\rm i}d^*_{m2} \\ \pm D^*_m - d^*_{m3} \end{pmatrix}, \tag{23}$$
$$\lambda_{m\pm} = d_{m0} \pm D_m, \tag{24}$$

where $D_m = \sqrt{d_{m1}^2 + d_{m2}^2 + d_{m3}^2}$. The winding number of eiganstates of $\tilde{U}'_m$ is defined by the global berry phase as

$$\nu'_m = \frac{\varphi_{m\rm B}}{2\pi}. \tag{25}$$

When m is even, we can redefine $\tilde{U}_m$ to be $\tilde{U}''_m$ in the other symmetric time frame, for example,

$$\tilde{U}''_4 = C\left(\frac{\theta_1}{2}\right) G^{-1} SC(\theta_1) SC(\theta_2) SC(\theta_1) GSC\left(\frac{\theta_1}{2}\right). \tag{26}$$

This redefined $\tilde{U}''_m$ also has PT symmetry and the PT operator is still $PT = \sum_x |-x\rangle\langle x| \otimes \sigma_z \mathcal{K}$. The corresponding winding number ν''_m is derived from the analogy of Eq. (28). By contrast, we cannot find the other symmetric time frame to define $\tilde{U}''_m$ when m is odd.

In the coin parameter space (θ_1, θ_2), the topological phase diagrams for the non-unitary three-period and four-period QWs are plotted in Figs. 2(a) and 2(b), respectively. The different topological phases are characterized by the winding number ν'_3 and (ν'_4, ν''_4), which are marked on the relevant phases of the figure. The shaded areas in the topological phase diagram are the domains where the PT symmetry is broken. The shaded area becomes larger and larger with the increasing gain loss coefficient γ. It is observed that the topological phase with a high winding number appears in our model. The value of ν'_3 is either ± 1 or ± 3. Here ν'_4 and ν''_4, which come from different symmetric time frames, have different ranges of values; ν'_4 may takes 0, ± 2 or ± 4; while ν''_4 takes 0 or ± 2. Besides relying on the choice of the symmetric time, the maximum value of high winding number is relative with the number of shift operation in one-step evolution. Generally, for the m-period quantum walk, the value of the winding number ν'_m may take ± 1, ± 3,..., $\pm m$ if m is odd; and take 0, ± 2, ± 4,..., $\pm m$ if m is even. However, the winding number ν''_m, which can be defined only if m is even, always takes 0, ± 2, in regardless of the value of m.

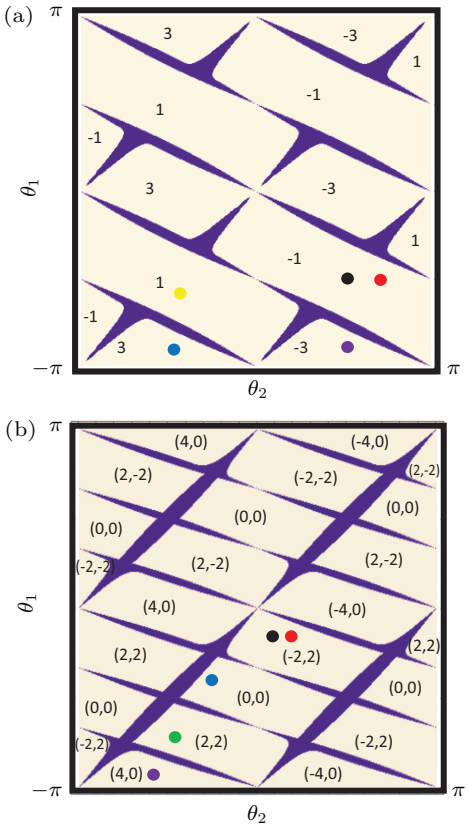


Fig. 2. Phase diagrams of (a) the non-unitary three-period quantum walk and (b) the non-unitary four-period quantum walk in coin parameter space (θ_1, θ_2) when $\gamma = 0.1$. Different topological phases are characterized by the winding numbers ν'_m in Fig. 1(a) and (ν'_m, ν''_m) in Fig. 1(b). The colored symbols indicate the coin parameters for observing the topological edge states.

The bulk–edge correspondence principle indicates that the difference in the winding numbers on either side of the boundary should be equal to the number of edge states.[28] To distinguish the edge state with ${\rm Re}(E_m) = 0$ (0-energy edge states) and the edge state with ${\rm Re}(E_m) = \pi$ (π-energy edge states), we introduce another definition of winding number for the even-period QW

$$(\nu^0_m, \nu^\pi_m) = \left(\frac{\nu'_m + \nu''_m}{2}, \frac{\nu'_m - \nu''_m}{2}\right). \tag{27}$$

The number of edge states with quasienergy ${\rm Re}(E_m) = 0$ (${\rm Re}(E_m) = \pi$) is equal to the difference of topological numbers ν^0_m (ν^π_m) on either side of the boundary. For the odd-period

QW, although we cannot find the other symmetric time frame to define U_m'' and v_m'', a definite result is that both 0-energy edge states and π-energy edge states occupy the topological phase boundary in Fig. 2(a) and the number of 0-energy edge states always equals that of π-energy edge states. The difference of v_m' on either side of phase boundary is the total number of two kinds of edge states. From the view of energy gap, the band gap closes at $\mathrm{Re}(E_m) = 0$ and π simultaneously, and the two kinds of topological numbers v_m^0 and v_m^π take the same value. Thus we do not distinguish the two kinds of topological numbers and denote them as v_m' for the odd-period QW. As a comparison, even 0-energy edge states and π-energy edge states coexist on the phase boundary for even-period QW, but the number of 0-energy edge states may not equal that of π-energy edge states, i.e., the difference of winding numbers v_m^0 may not equal that of v_m^π on either side of boundary.

3.3. Topological edge states

To verify the bulk–edge correspondence of the QW with high topological numbers, we still use the inhomogeneous three-period and four-period QW as an example. We consider the QW to be on a lattice with N sites and a periodic boundary condition is used. Take

$$\theta_{1(2)}(x) = \begin{cases} \theta_{1(2)}^{\mathrm{L}}, & N/2+1 \le x \le N, \\ \theta_{1(2)}^{\mathrm{R}}, & 1 \le x \le N/2, \end{cases} \tag{28}$$

where N is assumed to be an even number without losing generality. In the following, we take $N = 400$. The circular lattice have two boundaries near $x = 1$ and $x = N/2$ when $\theta_{1(2)}^{\mathrm{L}}$ and $\theta_{1(2)}^{\mathrm{R}}$ are different.

For the three-period QW, we fix $\left(\theta_1^{\mathrm{L}}, \theta_2^{\mathrm{L}}\right) = \left(-\frac{2\pi}{5}, \frac{2\pi}{5}\right)$ and consider several cases of $\left(\theta_1^{\mathrm{R}}, \theta_2^{\mathrm{R}}\right) = \left(-\frac{2\pi}{5}, \frac{3\pi}{5}\right)$, $\left(-\frac{4\pi}{5}, -\frac{3\pi}{5}\right)$, $\left(-\frac{4\pi}{5}, \frac{2\pi}{5}\right)$, $\left(-\frac{2\pi}{5}, -\frac{2\pi}{5}\right)$. In the phase diagram shown in Fig. 2(a), the positions of these parameter values are marked by the black circle dot, the red circle dot, the blue circle dot, the purple circle dot and the yellow circle dot, respectively. We calculate the eigenvalue of the evolution operator of this inhomogeneous QW, and its distributions in the complex plane are shown in Figs. 3(a)–3(d). Some isolated eigenvalues λ appear on the real axis in Figs. 3(b)–3(d) and consequently real part of the quasi-energy E_3 is 0 or π. In Fig. 3(a), there are no isolated eigenvalues on the real axis, which means that the edge state does not exist. As the same as the prediction of bulk–edge correspondence, the parameters of the coin at both sides of the boundary lead to the same topological phase with the topological number $v_3' = -1$ (see Fig. 2(a)).

Eight isolated eigenvalues with $\mathrm{Re}(E_3) = 0$ and π appear in Fig. 3(b). Figure 3(e) presents the corresponding eigenstates, two $0(\pi)$-energy edge states appear at the boundary $x = 0$ and two others appear at the boundary $x = N/2$, which illustrate that the number of 0-energy edge states equals that of π-energy edge states at each boundary for the odd-period QW as mentioned above. On the other hand, the winding numbers corresponding black circle dot and the blue circle dot in Fig. 2(a) are -1 and 3, respectively. The difference between them is $\delta v_3' = 4$. The total number of edge states at each boundary equals $\delta v_3'$, also satisfying the prediction of the bulk–edge correspondence.

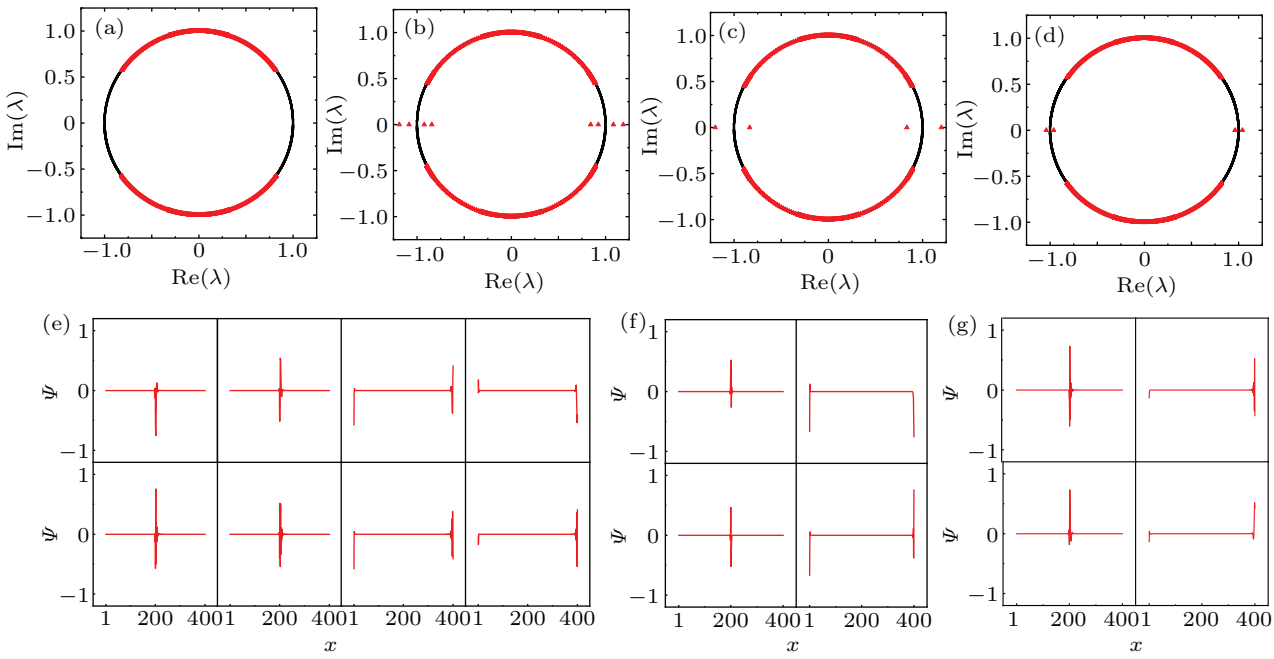


Fig. 3. The distributions of eigenvalue λ of the time-evolution operator $\tilde{U}_3$ are plotted in the complex plane for the case of (a) $\left(\theta_1^{\mathrm{R}}, \theta_2^{\mathrm{R}}\right) = \left(\frac{-2\pi}{5}, \frac{3\pi}{5}\right)$, (b) $\left(\theta_1^{\mathrm{R}}, \theta_2^{\mathrm{R}}\right) = \left(\frac{-4\pi}{5}, \frac{-3\pi}{5}\right)$, (c) $\left(\theta_1^{\mathrm{R}}, \theta_2^{\mathrm{R}}\right) = \left(\frac{-4\pi}{5}, \frac{2\pi}{5}\right)$ and (d) $\left(\theta_1^{\mathrm{R}}, \theta_2^{\mathrm{R}}\right) = \left(\frac{-2\pi}{5}, \frac{-2\pi}{5}\right)$. As a comparison, the black solid cycle represents an unit circle. Here, 0-energy edge states (top pattern) and π-energy edge states (bottom pattern) are shown in (e), (f) and (g), which are the eigenstates corresponding to the isolated eigenvalues in (b), (c) and (d), respectively.

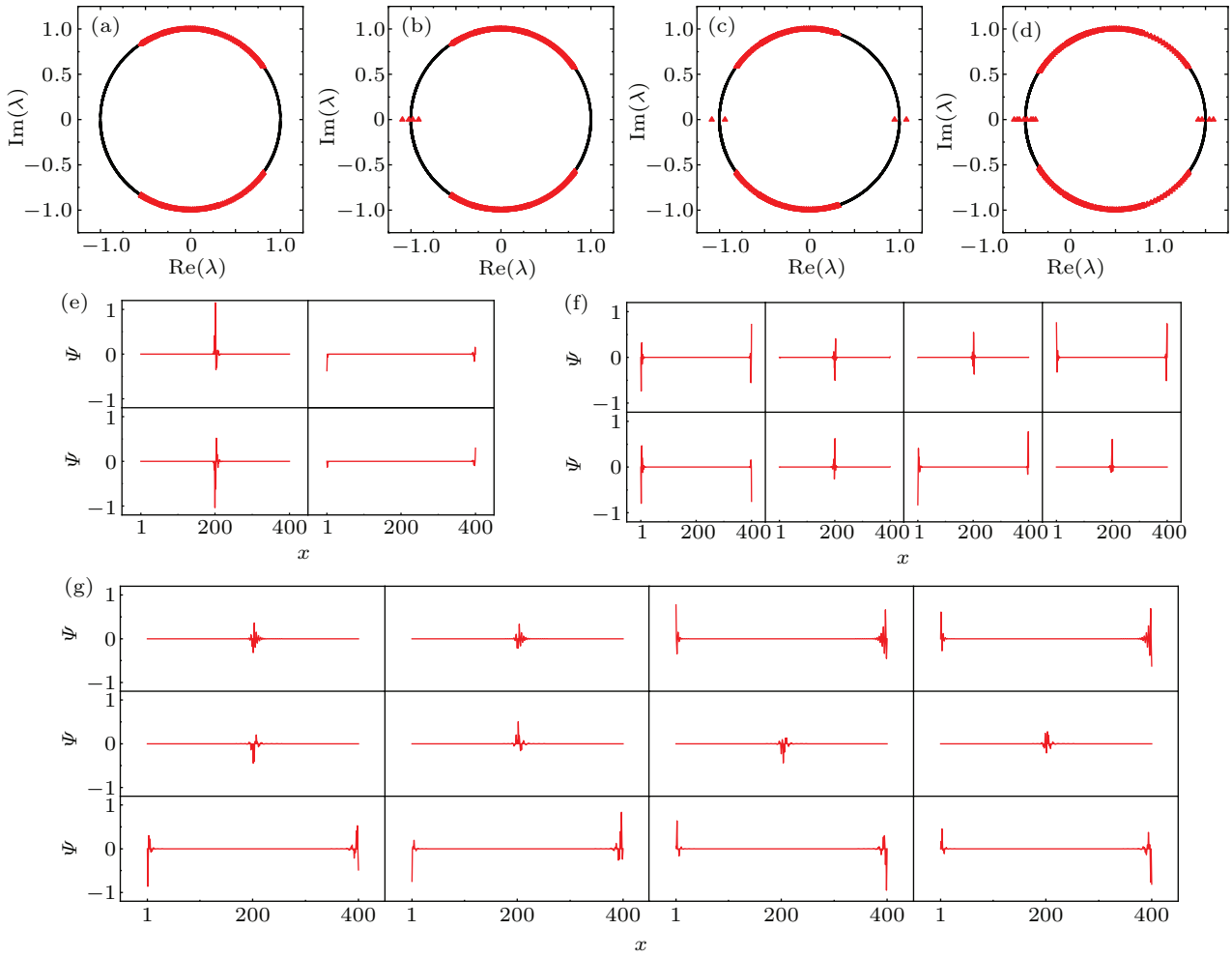


Fig. 4. The distributions of eigenvalue of the time-evolution operator are plotted in the complex plane for the cases of (a) $(\theta_1^{\mathrm{R}},\theta_2^{\mathrm{R}})=(\frac{-\pi}{5},\frac{2\pi}{5})$, (b) $(\theta_1^{\mathrm{R}},\theta_2^{\mathrm{R}})=(\frac{-2\pi}{5},\frac{-\pi}{5})$, (c) $(\theta_1^{\mathrm{R}},\theta_2^{\mathrm{R}})=(\frac{-4\pi}{5},\frac{-2\pi}{5})$ and (d) $(\theta_1^{\mathrm{R}},\theta_2^{\mathrm{R}})=(\frac{-\pi}{10},\frac{-3\pi}{5})$. The eigenstates corresponding to the isolated eigenvalue on the real axes of (b), (c) and (d) are shown in (e), (f) and (g), respectively. The entire subfigure (e), the top pattern of (f) and the top pattern of (g) show the 0-energy edge states, and the other patterns show the π-energy edge states.

Figure 3(c) includes four isolated eigenvalues with $\mathrm{Re}(E_3)=0$ and π. Two edge states with $\mathrm{Re}(E_3)=0$ and π exist at each boundary as shown in Fig. 3(f), which is consistent with the difference $\delta v_3'=2$ of the winding numbers marked by the black circle dot and the purple circle dot shown in Fig. 2(a). Due to the difference of the winding numbers marked by the black circle dot and the yellow circle dot in Fig. 2(a) also being $\delta v_3'=2$, Figs. 3(d) and 3(g) present the result similar to Figs. 3(c) and 3(f).

For the four-period QW, we also fix $(\theta_1^{\mathrm{L}},\theta_2^{\mathrm{L}})=(-\frac{\pi}{5},\frac{\pi}{5})$ and consider several cases of $(\theta_1^{\mathrm{R}},\theta_2^{\mathrm{R}})$ to be $(-\frac{\pi}{5},\frac{2\pi}{5})$, $(-\frac{2\pi}{5},-\frac{\pi}{5})$, $(-\frac{4\pi}{5},-\frac{2\pi}{5})$, $(-\frac{\pi}{10},-\frac{3\pi}{10})$. The coordinate positions of these parameter values are marked by the black circle dot, the red circle dot, the blue circle dot, the green circle dot and the purple circle dot, respectively, in Fig. 2(b). For such inhomogeneous coin parameters of Eq. (21), The eigenvalue distributions and the eigenstates corresponding to those isolated eigenvalues are plotted in Fig. 4.

For the case of $(\theta_1^{\mathrm{R}},\theta_2^{\mathrm{R}})=(-\frac{\pi}{5},\frac{2\pi}{5})$, there are no isolated eigenvalues in the real axis in Fig. 4(a). That is to say, there are no eigenstate located at the boundary. The coin parameters on both sides of the boundary belong to the same topological phase with the topological numbers $(\nu'_4,\nu''_4)=(-2,2)$, which also predicts that no edge state exists. Taking $(\theta_1^{\mathrm{R}},\theta_2^{\mathrm{R}})=(-\frac{2\pi}{5},-\frac{\pi}{5})$, Fig. 4(b) displays that four isolated eigenvalues with $\mathrm{Re}(E_4)=\pi$ are on the real axes. The corresponding four eigenstates are all π-energy edge states as shown in Fig. 4(e). Half of them locate at the boundary and the other half locate at the boundary $x=N/2$. The position of selected coin parameters $(\theta_1^{\mathrm{L}},\theta_2^{\mathrm{L}})$ and $(\theta_1^{\mathrm{R}},\theta_2^{\mathrm{R}})$ in Fig. 2(b) are marked by the black dot and the blue dot, where the winding numbers (ν'_4,ν''_4) are (−2,2) and (0,0), respectively. It is obvious that $\delta\nu_4^{\pi}=2$, the difference of winding numbers, is equal to the number of π-energy edge states at each boundary, and $\delta\nu_4^{0}=0$ is consistent with the case having no 0-energy edge states.

When taking $(\theta_1^{\mathrm{R}},\theta_2^{\mathrm{R}})=(\frac{-4\pi}{5},\frac{-2\pi}{5})$, the positions of two points $(\theta_1^{\mathrm{L}},\theta_2^{\mathrm{L}})$ and $(\theta_1^{\mathrm{R}},\theta_2^{\mathrm{R}})$ in Fig. 2(b) are marked by the black dot and the green dot. The differences of the winding numbers at these two positions are $\delta\nu_4^{0}=2$ and $\delta\nu_4^{\pi}=2$. For

this case, Fig. 4(c) shows that four isolated eigenvalues are on the real axes. They are all dually degenerate and the corresponding eigenstates are plotted in Fig. 4(f). Two 0-energy edge states and two π-energy edge states lie in each boundary. The numbers of the edge states are agreement with $\delta\nu_4^0 = 2$ and $\delta\nu_4^\pi = 2$.

Figures 4(d) and 4(g) with $\left(\theta_1^{\mathrm{R}}, \theta_2^{\mathrm{R}}\right) = \left(-\frac{\pi}{10}, -\frac{3\pi}{10}\right)$ present the interesting results. Eight isolated eigenvalues with $\mathrm{Re}(E_4) = \pi$ and four isolated eigenvalues with $\mathrm{Re}(E_4) = 0$ appear in Fig. 3(d). Four π-energy edge states and two 0-energy edge states exist at each boundary as shown in Fig. 3(f). Consistently, the difference of the winding numbers is $\delta\nu_4^0 = 2$ and $\delta\nu_4^\pi = 4$, for the black circle dot and the purple circle dot in Fig. 2(b). The feature that the number of 0-energy edge states does not equal that of π-energy edge states at each boundary is unique for the even-period QW. What is more, sometimes only 0-energy edge states or π-energy edge states locate at the boundary.

4. Conclusion

In summary, we construct a one-dimensional multi-period non-unitary QW with PT symmetry. For simplicity and without losing generality, we take a non-unitary three-period QW and a four-period QW as examples to investigate the topological characteristics, and topological phases with large topological invariants are obtained. The results can be generalized to two types of multi-period QW, old-period QW and even-period QW. The values of the winding number can take ±1, $\pm3,\ldots,\pm m$ for odd-period QW, and 0, ±2, $\pm4,\ldots,\pm m$ for even-period QW under appropriate time frame, where m is index of the m-period QW. Depending on the choice of time frame, the maximum of high winding number can reach the number of shift operations in one-step evolution.

The distinction of two types of the multi-period QW is that the band gap closes equivalently at $\mathrm{Re}(E_m) = 0$ and π for the odd-period QW, while the number of gap-closed line segments with $\mathrm{Re}(E_m) = 0$ and that with $\mathrm{Re}(E_m) = \pi$ may be unequal for the even-period QW. The validity of the bulk–edge correspondence is numerically confirmed, the number of multiple edge states agrees well with the difference in topological numbers. It is worth noting that 0-energy edge states and π-energy edge states only coexist equally on the boundary for the odd-period quantum walk. However, for the even-period quantum walk, 0-energy edge states and π-energy edge states can exist unequally or even only one kind of edge states exist on the boundary. Our research has deepened the understanding of topology phenomena with large topological invariants in non-unitary or non-Hermitian systems.

References

[1] Aharonov Y, Davidovich L and Zagury N 1993 *Phys. Rev. A* **48** 1687
[2] Kempe J 2003 *Contemp. Phys.* **44** 307
[3] Venegas-Andraca E S 2012 *Quantum Inf. Proc.* **11** 1015
[4] Tang B, Qin H, Zhang R, Liu J M and Xue P 2014 *Chin. Phys. B* **23** 050307
[5] Shenvi N, Kempe J and Birgitta Whaley K 2003 *Phys. Rev. A* **67** 052307
[6] Kitagawa T, Rudner M S, Berg E and Demler E 2010 *Phys. Rev. A* **82** 033429
[7] Kurzyński P and Wójcik A 2011 *Phys. Rev. A* **83** 062315
[8] Kitagawa T *et al.* 2010 *Phys. Rev. A* **82** 033429
[9] Groh T, Brakhane S, Alt W *et al.* 2016 *Phys. Rev. A* **94** 013620
[10] Zhan X, Xiao L, Bian Z, Wang K, Qiu X, Sanders B C, Yi W and Xue P 2017 *Phys. Rev. Lett.* **119** 130501
[11] Rakovszky T and Asboth J K 2015 *Phys. Rev. A* **92** 052311
[12] Panahiyan S and Fritzsche S 2019 *Phys. Rev. A* **100** 062115
[13] Du J, Li H, Xu X, Shi M, Wu J, Zhou X and Han R 2003 *Phys. Rev. A* **67** 042316
[14] Ryan C A, Laforest M, Boileau J C and Laflamme R, E 2005 *Phys. Rev. A* **72** 062317
[15] Lu D W *et al.* 2016 *Phys. Rev. A* **93** 042302
[16] Genske M, Alt W, Steffen A, Werner A H, Werner R F, Meschede D and Alberti A 2013 *Phys. Rev. Lett.* **110** 190601
[17] Robens C, Alt W, Meschede D, Emary C and Alberti A 2015 *Phys. Rev. X* **5** 011003
[18] Peruzzo A *et al.* 2010 *Science* **329** 1500
[19] Xue P, Qin H, Tang B, Zhan X, Bian Z H and Li J 2014 *Chin. Phys. B* **13** 110307
[20] Schreiber A *et al.* 2011 *Phys. Rev. Lett.* **106** 180403
[21] Jeong Y C, Franco C D, Lim H T, Kim M S and Kim Y H 2013 *Nat. Commun.* **4** 2471
[22] Zeuner J M, Rechtsman M C, Plotnik Y, Lumer Y, Nolte S, Rudner M S, Segev M and Szameit A 2015 *Phys. Rev. Lett.* **115** 040402
[23] Zhan X, Xiao L, Bian Z H, Wang K K, Qiu X Z, Sanders B C, Yi W and Xue P 2017 *Phys. Rev. Lett.* **119** 130501
[24] Xiao L, Zhan X, Bian Z H, Wang K K, Zhang X, Wang X P, Li J, Mochizuki K, Kim D, Kawakami N, Yi W, Obuse H, Sanders B C and Xue P 2017 *Nat. Phys.* **13** 1117
[25] Zhang R, Liu Y F and Chen T 2020 *Phys. Rev. A* **102** 022218
[26] Weimann S, Kremer M, Plotnik Y, Lumer Y, Nolte S, K, Makris K G, Segev M, Rechtsman M C and Szameit A 2017 *Nat. Mater.* **16** 433
[27] Poli C, Bellec M, Kuhl U, Mortessagne F and Schomerus H 2015 *Nat. Commun.* **6** 6710
[28] Asboth J K 2013 *Phys. Rev. B* **88** 121406
[29] Tarasinski B, Asboth J K and Dahlhaus J P 2014 *Phys. Rev. A* **89** 042327
[30] Gong Z, Ashida Y, Kawabata K, Takasan K, Higashikawa S and Ueda M 2018 *Phys. Rev. X* **8** 031079
[31] Kawabata K, Shiozaki K and Ueda M and Sato M 2018 *Phys. Rev. X* **9** 041015
[32] Xiao L, Qiu X, Wang K K, Bian Z, Zhan X, Obuse H, Sanders B C, Yi W and Xue P 2018 *Phys. Rev. A* **98** 063847
[33] El-Ganainy R, Markris K G, Khajavikhan M *et al.* 2018 *Nat. Phys.* **10** 1038
[34] Bender C M and Boettcher S 1998 *Phys. Rev. Lett.* **80** 5243